

Massive Black Hole Binaries from the TNG50-3 Simulation: II. Using Dual AGNs to Predict the Rate of Black Hole Mergers

KUNYANG LI ¹, TAMARA BOGDANOVIĆ ¹, DAVID R. BALLANTYNE ¹ AND MATTEO BONETTI ^{2,3}

¹*School of Physics and Center for Relativistic Astrophysics, 837 State St NW, Georgia Institute of Technology, Atlanta, GA 30332, USA*

²*Dipartimento di Fisica G. Occhialini, Università di Milano-Bicocca, Piazza della Scienza 3, IT-20126 Milano, Italy*

³*INFN, Sezione di Milano-Bicocca, Piazza della Scienza 3, IT-20126 Milano, Italy*

Submitted to ApJ

ABSTRACT

Dual active galaxy nuclei (dAGNs) trace the population of post-merger galaxies and are the precursors to massive black hole (MBH) mergers, an important source of gravitational waves that may be observed by *LISA*. In Paper I of this series, we used the population of ≈ 2000 galaxy mergers predicted by the TNG50-3 simulation to seed semi-analytic models of the orbital evolution and coalescence of MBH pairs with initial separations of ≈ 1 kpc. Here, we calculate the dAGN luminosities and separation of these pairs as they evolve in post-merger galaxies, and show how the coalescence fraction of dAGNs changes with redshift. We find that because of the several Gyr long dynamical friction timescale for orbital evolution, the fraction of dAGNs that eventually end in a MBH merger grows with redshift and does not pass 50% until $z_{\text{dAGN}} \approx 1$. However, dAGNs in galaxies with bulge masses $\lesssim 10^{10} M_{\odot}$, or comprised of near-equal mass MBHs, evolve more quickly and have higher than average coalescence fractions. At any redshift, dAGNs observed with small separations ($\lesssim 0.7$ kpc) have a higher probability of merging in a Hubble time than more widely separated systems. As found in Paper I, radiation feedback effects can significantly reduce the number of MBH mergers, and this could be manifested as a larger than expected number of widely separated dAGNs. We present a method to estimate the MBH coalescence rate as well as the potential *LISA* detection rate given a survey of dAGNs. Comparing these rates to the eventual *LISA* measurements will help determine the efficiency of dynamical friction in post-merger galaxies.

Keywords: galaxies: evolution — galaxies: kinematics and dynamics — galaxies: nuclei — quasars: super-massive black holes

1. INTRODUCTION

Dual Active Galactic Nuclei (dAGNs) are two accreting massive black holes (MBHs) residing within a single host galaxy and are expected to occur following the merger of two massive galaxies. A population of dAGNs in post-merger galaxies seems to be an unavoidable prediction of hierarchical galaxy formation models (e.g. De Rosa et al. 2020). In some cases, the separation of the two MBHs that comprise a dAGN will shrink slowly over time as the orbiting MBHs interact

with the gaseous and stellar backgrounds of the galaxy (e.g., Begelman et al. 1980; Volonteri et al. 2003; Barausse 2012; Valiante et al. 2016; Bonetti et al. 2019; Khan et al. 2019; Li et al. 2022), eventually leading to the emission of gravitational waves and the coalescence of the two black holes (e.g., Amaro-Seoane et al. 2017; Kelley et al. 2017, 2019). Therefore, dAGNs are ‘tracers’ of future MBH mergers and gravitational wave events. An observed sample of dAGNs, combined with a model describing their future evolution, can thus provide a prediction of the MBH merger rate, a critical parameter for the upcoming *Laser Interferometer Space Antenna (LISA)* gravitational wave observatory.

Whether an observable dAGN results in a MBH coalescence depends on the physical processes within the remnant galaxy that drive the orbital evolution of the MBHs. When the MBHs are at separations of ~ 1 kpc, dynamical friction (DF) by gas and stars is expected to dominate the orbital de-

kli356@gatech.edu

tamarab@gatech.edu

david.ballantyne@physics.gatech.edu

matteo.bonetti@unimib.it

cay (Begelman et al. 1980). In this process, gravitational deflection of gas (Ostriker 1999; Kim & Kim 2007) or collisionless particles (e.g., stars and dark matter; Chandrasekhar 1943; Antonini & Merritt 2012) causes an overdense wake to form behind each MBH. The wakes exert a gravitational pull onto the MBHs, which saps their orbital energy. Once the two MBHs are gravitationally bound (at separations \sim pc) stellar “loss-cone” scattering is expected to dominate the orbital decay (e.g., Quinlan 1996; Quinlan & Hernquist 1997; Yu 2002). If the galaxy is sufficiently gas rich, drag on the binary by the surrounding circumbinary disk may also affect its orbital evolution at separations \lesssim 0.1 pc (e.g., Armitage & Natarajan 2005; Milosavljević & Phinney 2005). Only when the separation falls below \sim 1000 Schwarzschild radii does gravitational wave emission begin to dominate the orbital evolution until the MBHs merge (e.g., Thorne & Braginskii 1976; Begelman et al. 1980). In addition to the orbital decay, the gas content of the post-merger galaxy will also strongly influence the accretion rates onto the MBHs and their subsequent properties as dAGNs. As a result, connecting observations of dAGNs to their potential future gravitational wave sources will depend on the properties of the host galaxy and the orbit of the MBH pair (e.g., Li et al. 2021).

In Paper I of this series (Li et al. 2022), we presented the results of a semi-analytic model that followed the dynamical evolution of \approx 8000 MBH pairs from \sim 1 kpc to coalescence accounting for all the processes described above (DF, loss-cone scattering, decay in a circumbinary disk, and gravitational wave emission). The host galaxy models in which the MBH pairs evolved were constructed from the properties of merger galaxies in the TNG50-3 cosmological simulation (Nelson et al. 2019a,b; Pillepich et al. 2019). Paper I showed that the DF phase was the most important process in determining if a MBH pair would coalesce within a Hubble time, and therefore the stellar and gas content at scales of a few hundreds pc in post-merger galaxies are critical for the expected *LISA* detection rates. Moreover, we found that radiation feedback effects from the accreting MBHs has the potential to significantly weaken DF forces in gas-rich galaxies (e.g., Park & Bogdanović 2017; Li et al. 2020a), which could severely reduce the number of MBH mergers detected by *LISA*. It is crucial, therefore, to find a method that can test these predictions, especially the potential role of radiation feedback, and observationally constrain the *LISA* expectations.

Here, we build on the results of Paper I by describing the expected dAGN properties of MBH pairs as they evolve towards coalescence. Paper I shows that the galaxy properties at \sim 1 kpc scale are often crucial for the overall orbital decay, and so we focus on the dAGN properties with separations in this range. As our model follows these MBH pairs through to coalescence, we demonstrate that observational surveys of dAGNs can provide an estimate of the expected MBH merger rate. Crucially, we consider the impact of radiation feedback on both the dynamics and accretion onto the MBHs, allowing for an observational determination of the magnitude of this effect.

This paper is organized as follows. In § 2 we provide a brief summary of the main features of the calculation used to evolve the MBHs and how the TNG50-3 simulation data is used as input to the model. § 3 shows how the distributions of dAGN luminosity and separation change over time. § 4 presents the merger fraction of dAGNs at different redshifts and how this depends on the properties of the host galaxy and MBH pair. The impact of radiation feedback on these results is shown in § 5. Finally, we discuss the implications of our findings in § 6 and conclude in § 7. We assume a cosmology consistent with that used in the TNG50-3 simulation ($\Omega_{\Lambda,0} = 0.6911$, $\Omega_{m,0} = 0.3089$, $\Omega_{b,0} = 0.0486$, $h = 0.6774$), and $t_{\text{Hubble}} = 14.4$ billion yrs.

2. METHODS

A thorough description of the dynamical evolution calculation of MBH pairs and our use of the TNG50-3 simulation data is found in Paper I (see also Li et al. 2020b). We therefore provide a brief summary of the method below before describing how we compute the time-dependent accretion rate and luminosity of each of our model dAGNs.

2.1. The Dynamical Evolution of MBH Pairs in TNG50-3 Post-Merger Galaxies

We assume that a galaxy merger produces a single remnant, with a stellar bulge and gas disk¹, which includes the MBH pair. The primary MBH (pMBH; with mass M_1) is fixed at the center of the galaxy. The non-rotating bulge has a mass M_{sb} and follows a coreless powerlaw density profile (e.g., Binney & Tremaine 2008), which is cutoff at twice the half-mass radius of the bulge ($2 \times R_{\text{b,h}}$), with the scale parameters proportional to $\log(M_1/10^5 M_{\odot})$ kpc. We consider the orbital evolution of a bare, secondary MBH (sMBH; with mass $M_2 < M_1$) which is orbiting in the plane of the gas disk. The total mass of the MBH pair is $M_{\text{bin}} = M_1 + M_2$ and the mass ratio is $q = M_2/M_1$.

The gas fraction of the remnant galaxy is $f_g = M_{\text{gd}}/(M_{\text{gd}} + M_{\text{sb}})$, where M_{gd} is the mass of the gas disk within twice the half-mass radius of the gas disk ($2 \times R_{\text{g,h}}$). Once f_g is set the gas densities are determined using an exponential profile with a scale radius defined as $2 \log(M_1/10^5 M_{\odot})$ kpc (e.g., Binney & Tremaine 2008). As a result, galaxies with a larger pMBH have gas densities that decrease more slowly with radius. The gas disk of each galaxy rotates with a speed drawn from the uniform distribution $0.7 - 0.9 v_c(r)$, where $v_c(r)$ is the local circular velocity.

A list of 1997 galaxy merger events, including redshifts and MBH masses, is extracted from the catalogs of the TNG50-3 simulation². Specifically, the redshifts correspond to when the two MBHs reach a separation equal to the gravitational softening length of the collisionless component (\approx 1 kpc). The properties of the remnant galaxy (M_{sb} , M_{gd} ,

¹ We neglect the stellar disk in the calculation as its impact on the orbital evolution of an MBH is relatively minor (Li et al. 2020b).

² See <https://www.tng-project.org/data/docs/specifications>

$R_{b,h}$, and $R_{g,h}$) are also extracted from the TNG50-3 catalogs and are used to construct the galaxy model within which the MBH pair evolves. The dynamical evolution of the pair is initialized so that the semi-major axis a is ≈ 1 kpc. The initial eccentricity of the sMBH is set to be either $e_i < 0.2$ or $0.8 \leq e_i \leq 0.9$, and we consider both prograde and retrograde orbits (Li et al. 2020b). Thus, we compute four distinct evolutions of the sMBH in each of the 1997 post-merger galaxies. The results presented below are from the combined dataset of 7988 calculations.

The orbital evolution of the sMBH due to DF is computed as described by Li et al. (2020b,a). This process takes the sMBH down to the influence radius of the MBH pair, where the mass enclosed by the orbit is equal to twice the pair mass. Below this radius, the orbital decay is due to the combination of loss-cone scattering, drag from the circumbinary gas disk, and gravitational wave emission. The calculation ends when the orbital separation is smaller than the radius of the innermost stable circular orbit (ISCO) of a non-spinning MBH pair (i.e., $R_{\text{ISCO}} = 6GM_{\text{bin}}/c^2$). Paper I provides full details of how the orbital evolution is computed below the influence radius. The full decay time of the sMBH is tracked and the MBH coalescence redshift, z_{coal} , is recorded for each calculation that merges within a Hubble time (36% of the 7988 orbital evolutions do not successfully merge within this time; see § 3 of Paper I).

Lastly, for those models which successfully reach coalescence, we compute the expected *LISA* signal-to-noise ratio (SNR) during the inspiral phase assuming a four-year mission lifetime (Appendix A of Paper I; Bonetti et al. 2019). The detection threshold for *LISA* used in this paper is a $\text{SNR} > 8$. This information will allow us to connect *LISA*-detectable MBH pairs to their earlier dAGN properties.

2.2. Accretion Rates and Luminosities

The accretion rates onto both the pMBH and sMBH are calculated as a function of time during the DF phase of the calculation. That is, we compute the dAGN luminosities only when the separations are greater than the influence radius of the MBH pair (~ 1 pc). For simplicity, we neglect the mass increase of each MBH due to accretion and consider only bolometric luminosities (see § 6).

The accretion rate onto the stationary pMBH is computed using the Bondi formula (Bondi & Hoyle 1944; Bondi 1952) and its luminosity is limited to be no more than 10% of the Eddington luminosity (e.g., Lusso et al. 2012), i.e.,

$$L_1 = \begin{cases} 0.1\dot{M}_{B1}c^2 & \text{when } L_1 < 0.1L_{1,\text{Edd}}, \\ 0.1L_{1,\text{Edd}} & \text{otherwise,} \end{cases} \quad (1)$$

where $\dot{M}_{B1} = \pi n_{\text{gd}0} m_{\text{p}} (GM_1)^2 / c_{\text{s}1,\infty}^3$ is the Bondi accretion rate onto the pMBH and $L_{1,\text{Edd}} = 4\pi GM_1 m_{\text{p}} c / \sigma_{\text{T}}$ is its Eddington luminosity. In the Bondi formula $n_{\text{gd}0}$ is the central gas density and $c_{\text{s}1,\infty}$ is the sound speed at the galactic center. To determine the sound speed, the temperature profile of the gas disk is assumed to be 10^4 K above the minimum Toomre stability temperature (Toomre 1964).

As the sMBH is moving through the post-merger galaxy, its accretion rate is calculated using the Bondi-Hoyle-Lyttleton model, which accounts for the drop in accretion due to the relative motion of the MBH (Hoyle & Lyttleton 1939; Bondi & Hoyle 1944; Bondi 1952), $\dot{M}_{\text{BHL}} = \dot{M}_{\text{B}2} / (1 + \Delta v^2 / c_{\text{s}2,\infty}^2)^{3/2}$. Here, $\dot{M}_{\text{B}2}$ represents the regular Bondi rate of the sMBH, $c_{\text{s}2,\infty}$ is the sound speed of the gas at the same radius as the sMBH, and Δv is the velocity of the sMBH relative to the gas disk. The resulting accretion luminosity of the sMBH is

$$L_2 = \begin{cases} 0.1\dot{M}_{\text{BHL}}c^2 & \text{when } L_2 < L_{2,\text{Edd}}, \\ L_{2,\text{Edd}} & \text{otherwise,} \end{cases} \quad (2)$$

where $L_{2,\text{Edd}} = 4\pi GM_2 m_{\text{p}} c / \sigma_{\text{T}}$ is the Eddington luminosity of the sMBH.

The dependence of L_2 on both gas density and relative velocity means that the AGN luminosity of the sMBH may vary significantly during each orbit and will also show a long-term evolution as the orbit decays. Therefore, we expect the properties of the dAGN population to change with redshift as MBH pairs evolve in time (see also Li et al. 2021). In this paper, we do not consider the instantaneous luminosity of dAGNs, instead, we use the evolution time weighted luminosity, which is calculated by summing the product of the instantaneous luminosity and the time step through the entire evolution, and then divide it by total evolution time.

To summarize, we have computed the full dynamical evolution (from separations of ≈ 1 kpc to coalescence) of 7988 MBH pairs evolving in model post-merger galaxies derived from the TNG50-3 simulation. We also compute the *LISA* SNR for those pairs that successfully merge within a Hubble time. As described above, we also track estimates of the dAGN luminosities of each pair while their separations are $\gtrsim 1$ pc. In the rest of the paper, we explore the connections between dAGNs and MBH merger events. To do so, we define z_{dAGN} as the redshift at which a dAGN is observed and z_{coal} as the redshift at which the two MBHs that comprise the dAGN eventually coalesce (where $z_{\text{coal}} < z_{\text{dAGN}}$). The luminosity of a dAGN is defined as $L_{\text{bol}} = L_1 + L_2$.

3. THE EVOLUTION OF DUAL ACTIVE GALACTIC NUCLEI LUMINOSITIES AND SEPARATIONS

In this section we provide an overview of the evolving dAGN population found in our model suite. TNG50-3 predicts a small number of galaxy mergers beyond a redshift of 3 (Fig. 2 in Paper I), so we limit our analysis of dAGNs to lower redshifts (in particular, $z_{\text{dAGN}} \leq 2$) where the population of dAGNs is largest.

The minimum MBH mass in the TNG50-3 simulation is $\approx 10^6 M_{\odot}$ (Nelson et al. 2019b), which means that the lower-limit to the dAGN luminosity distribution is $L_{\text{bol}} \approx 10^{43} \text{ erg s}^{-1}$ (i.e., the maximum allowed luminosity of a pMBH with this mass; Eq. 1). The solid green histogram in Figure 1 shows how the total population of model dAGNs with $L_{\text{bol}} > 10^{43} \text{ erg s}^{-1}$ evolves with z_{dAGN} . Since the orbital evolution time of a dAGN in the DF phase is frequently

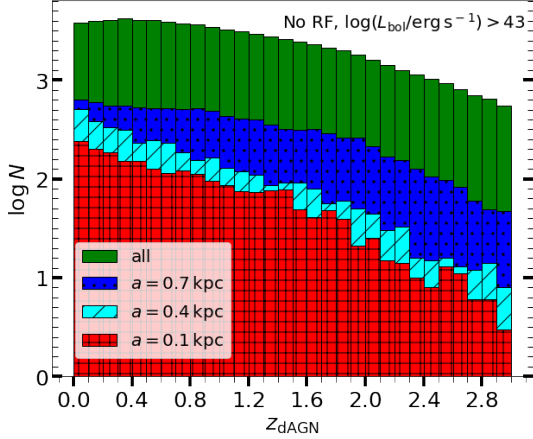


Figure 1. The redshift distribution of all dAGNs with total bolometric luminosity larger than 10^{43} erg s^{-1} and with separations of 0.7, 0.4, and 0.1 kpc.

> 1 Gyr (Paper I), one system can appear in multiple redshift bins as long as its $L_{\text{bol}} > 10^{43}$ erg s^{-1} in that redshift range. We find that the largest number of dAGNs are present in the redshift range of 0.4 – 0.5, and the number drops as the redshift increases from 0.5 to 3. The distribution of DF evolution times and galaxy gas fractions combine to determine this redshift distribution. Paper I showed that the evolution time for a sMBH to reach $a \sim 0.001$ kpc from $a \sim 1$ kpc ranges from ~ 1 Gyr (if the stellar bulge dominates) to $\sim 5 - 10$ Gyr (if the gas disk dominates) depending on the orbital configuration of the sMBH. Thus, only the systems containing dAGNs whose orbital evolution is determined by stellar DF in the bulge and have relatively short evolution time will evolve to pc-scales at high z_{dAGN} . The dAGNs whose orbital evolution is determined by the slower gaseous DF process reaches this separation at lower redshifts.

Fig. 1 also illustrates the redshift distribution of dAGNs with separations of 0.7, 0.4 and 0.1 kpc. All three distributions peak at the smallest redshifts $z_{\text{dAGN}} \approx 0-0.1$, but the peak is flattest and the total number of dAGNs highest for $a = 0.7$ kpc. This is because there are always more dAGNs with large rather than with small separations. This happens because all dAGNs with small separations were once dAGNs with large separations in the past, but not all dAGNs with large separations evolve into dAGNs with small separations. Taking everything into account, the shape of the redshift distribution of dAGNs is a natural result of DF dominated orbital evolution. This slow evolution means that $z_{\text{dAGN}} \lesssim 0.5$ is the optimal region for observational searches for dAGNs.

Turning now to the 65% of dAGNs that eventually lead to a MBH merger, Figure 2 shows the separation and luminosity distributions at $z_{\text{dAGN}} = 0.1, 1$ and 2 of all dAGN that will coalesce (solid blue histograms). The total number of dAGNs at $z_{\text{dAGN}} = 1$ and 2 that eventually merge is larger than that at $z_{\text{dAGN}} = 0.1$ because MBH mergers can happen

between $z_{\text{dAGN}} = 1$ and 0.1 and these do not appear in the leftmost distribution. The top three panels of Fig. 2 show that most dAGNs at $z_{\text{dAGN}} = 1$ and 2 that eventually merge have separations in the range of 0.5 – 1 kpc. This is because the evolution time from ~ 1 kpc to coalescence is often in the range of 5 – 10 Gyrs (Paper I). The separation distribution at $z_{\text{dAGN}} = 2$ (the rightmost panel) has a secondary peak at $a \sim 1.2$ kpc. This is because the time between $z_{\text{dAGN}} = 2$ and 0 (≈ 10 Gyrs) is long enough to allow some MBH pairs with separations larger than 1 kpc to merge within a Hubble time. The peak of the distribution at $z_{\text{dAGN}} = 0.1$ is shifted towards 0.2 – 0.5 kpc due to the relatively short evolution time between $z_{\text{dAGN}} = 0.1$ and 0 (~ 1 Gyr).

The solid blue histograms in the bottom three panels of Fig. 2 show the distribution of L_{bol} for all dAGNs at $z_{\text{dAGN}} = 0.1, 1$, and 2 whose MBHs merge before $z_{\text{coal}} = 0$. As expected, there is a sharp cutoff at $L_{\text{bol}} \approx 10^{43}$ erg s^{-1} due to the minimum MBH mass in the TNG50-3 simulation. At all z_{dAGN} the majority of dAGNs that eventually merge have $L_{\text{bol}} \approx 10^{43-45}$ erg s^{-1} .

The hatched red histograms in Fig. 2 shows the distributions of dAGNs that lead to $LISA$ SNR > 8 . These potential $LISA$ sources follow a similar trend in the separation distribution at all three redshifts. However, at luminosities larger than $\approx 10^{45}$ erg s^{-1} , the fraction of $LISA$ sources drops significantly in the lower three panels. This is because the bolometric luminosity is proportional to the binary mass, so more luminous precursor dAGNs have more massive MBHs and are less likely to be detected by $LISA$.

4. THE COALESCENCE FRACTION OF KPC-SCALE DUAL ACTIVE GALACTIC NUCLEI

This section presents the coalescence fraction of dAGNs as a function of redshift and observable properties of dAGN hosts. These fractions provide a quantitative relation between the number of dAGNs and merging MBHs, and can be used to estimate the cosmological MBH binary coalescence rate and the number of $LISA$ detections from a sample of detected dAGNs.

4.1. The Coalescence Fraction As a Function of Dual AGN Redshift

In order to quantify the relationship between observable dAGNs and MBH coalescence, we count the number of dAGNs with $L_{\text{bol}} > 10^{43}$ erg s^{-1} with MBHs that coalesce before $z_{\text{coal}} = 0$ and show the coalescence fraction as a function of z_{dAGN} in the left panel of Figure 3, grouped by dAGN separation. Almost all dAGNs with $a = 0.1$ kpc at $z_{\text{dAGN}} > 0.1$ eventually coalesce by $z_{\text{coal}} = 0$. The evolution time of these systems is 10^5-8 yrs (Paper I), which is sufficient for a dAGN with a separation of $a = 0.1$ kpc at $z_{\text{dAGN}} = 0.1$ to coalesce (the corresponding cosmological time is ~ 1.3 Gyr). Thus, if a dAGN is observed with $a \leq 0.1$ kpc at any redshift larger than 0.1, then it has nearly 100% chance to coalesce in a Hubble time.

Similarly, all dAGNs with $a = 0.4$ kpc at $z_{\text{dAGN}} > 0.4$ coalesce before $z_{\text{coal}} = 0$, but the coalescence fraction be-

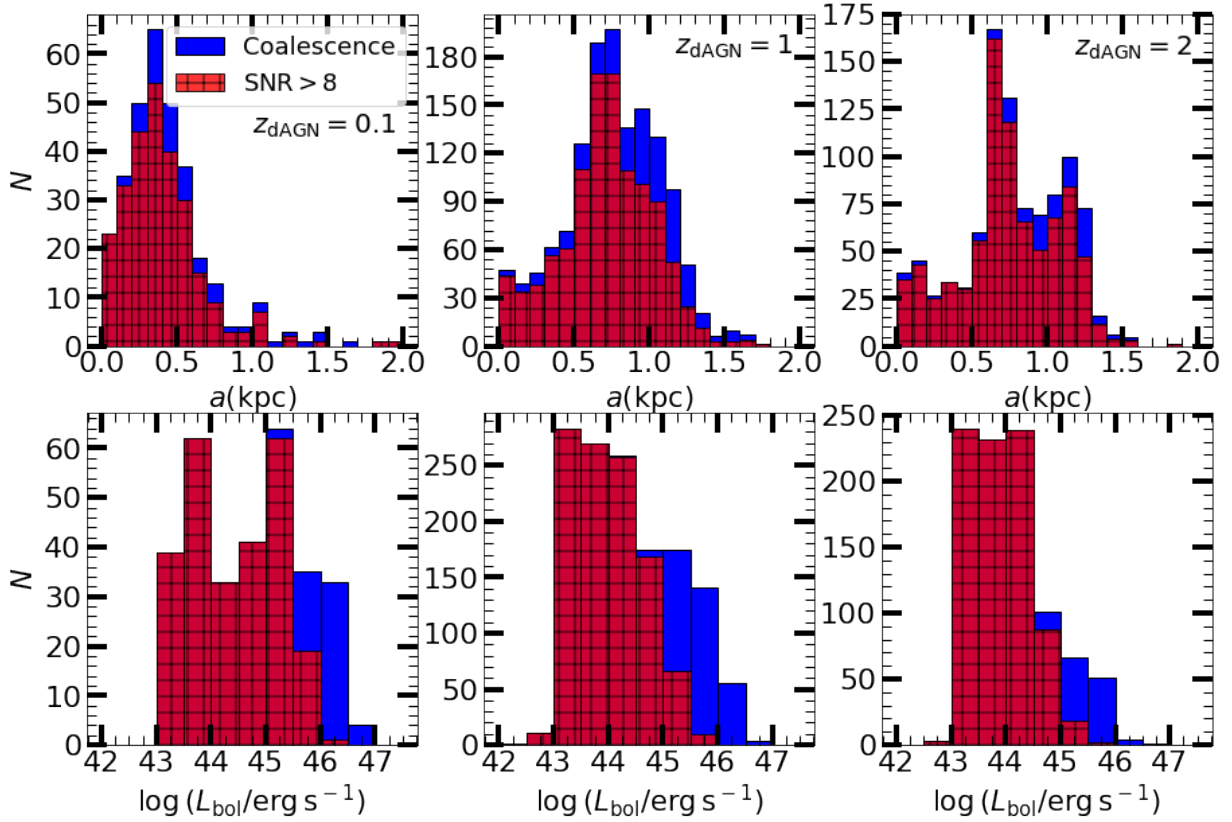


Figure 2. The separation and luminosity distributions at $z_{\text{dAGN}} = 0.1, 1,$ and 2 of dAGNs whose MBHs coalesce by $z_{\text{coal}} = 0$. The blue solid histograms show all dAGNs that eventually lead to coalescence by $z_{\text{coal}} = 0$, and the red hatched histograms show the systems in which the MBH merger has a *LISA* SNR > 8 .

tween $z_{\text{dAGN}} = 0$ and 0.1 drops to ~ 0.3 , showing that majority of these systems have an evolution time longer than ~ 1.3 Gyrs. The coalescence fraction of dAGNs with separations of 0.7 kpc gradually increases as redshift grows. This is as expected, since higher redshift dAGNs that reach separations of $a = 0.7$ kpc have a greater probability to evolve to coalescence prior to $z_{\text{coal}} = 0$. Indeed, the left panel of Fig. 3 shows that nearly 90% of dAGNs with $a = 0.7$ kpc at $z_{\text{dAGN}} = 3$ lead to a MBH merger. However, this fraction drops to 50% at $z_{\text{dAGN}} = 0.3$. The coalescence fraction of dAGNs with separations of $a = 0.7$ kpc is in general lower than those with $a = 0.1$ or 0.4 kpc because it is easier for the sMBH to evolve to coalescence from 0.1 kpc than from 0.7 kpc.

The coalescence fraction of all dAGNs with $L_{\text{bol}} > 10^{43}$ erg s^{-1} is shown as the red circles in Fig. 3 and is $\sim 70\%$ at $z_{\text{dAGN}} = 3$ and $\sim 50\%$ at $z_{\text{dAGN}} = 1$. Thus, given a sample of $z_{\text{dAGN}} = 1$ dAGNs with $L_{\text{bol}} > 10^{43}$ erg s^{-1} with separations of $0.001 - 2$ kpc, we expect that half of them will coalesce before $z_{\text{coal}} = 0$. In order to estimate the number of potential *LISA* sources using the number of observed dAGNs, we also count the number of dAGN that coalesce be-

fore $z_{\text{coal}} = 0$ with *LISA* SNR > 8 , and show this fraction as black plus signs in the left panel of Figure 3. As expected, the *LISA* detectable fraction is lower than the coalescence fraction at all redshifts, since *LISA* will not be as sensitive to the most massive MBH pairs.

Since the evolution time of the sMBH depends on the properties of the post-merger galaxy and MBH pair (Li et al. 2020b, Paper I), Figure 4 shows how the coalescence fraction of dAGNs is impacted by the galaxy bulge mass (left panel) and the MBH binary mass ratio (right panel). We find that the coalescence fraction of dual AGNs is inversely proportional to M_{sb} , with the largest fractions in galaxies with bulge masses of $M_{\text{sb}} \approx 10^9 M_{\odot}$ and the lowest with $M_{\text{sb}} \approx 10^{11} M_{\odot}$. This is a result of the inverse relationship between M_{sb} and f_g (§ 2.1) so that galaxy models with less massive bulges have higher gas fraction (and, thus, high gas densities and sound speeds), where gaseous DF efficiently decays the orbit of the sMBH at large separations (see also Paper I). When $M_{\text{sb}} > 10^{10} M_{\odot}$, the gas fraction falls to low enough values that gaseous DF becomes inefficient, increasing the decay time of the sMBH before the stellar DF can take over. The coalescence fractions of the

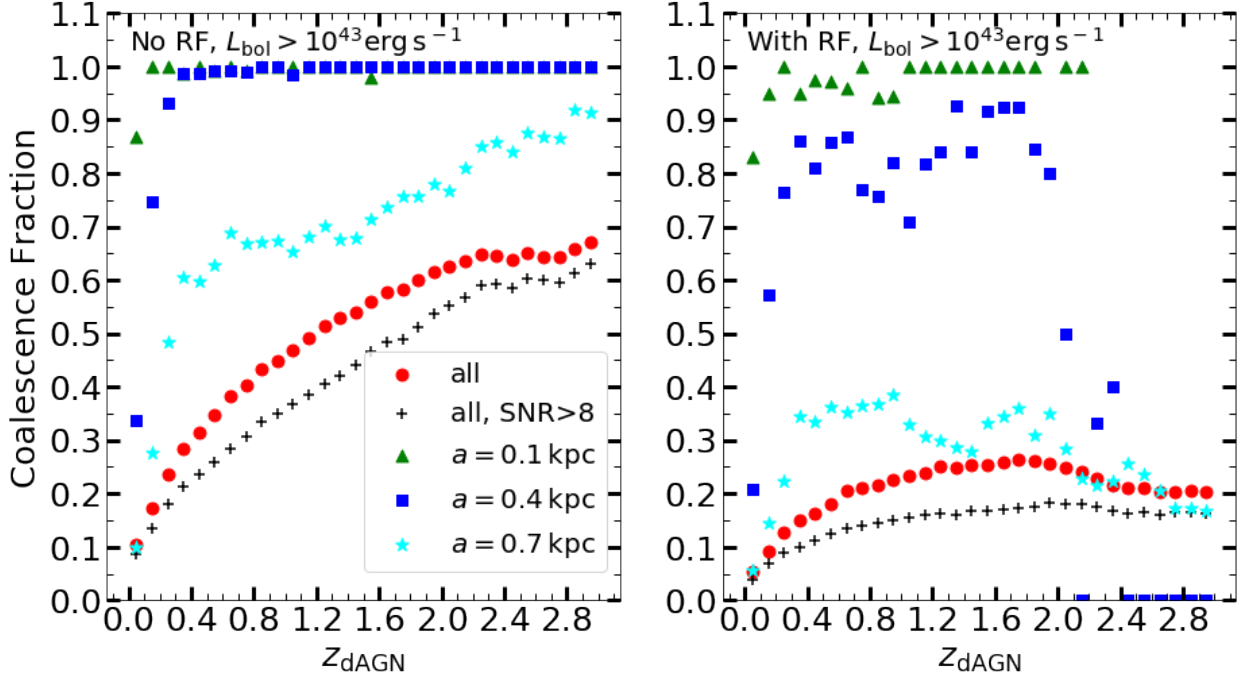


Figure 3. The fraction of dAGNs observed at a given redshift whose MBHs coalesce before $z_{\text{coal}} = 0$. The red circles show the fraction using all 7988 dAGNs in the model suite, while the green triangles, blue squares and cyan stars show how the fraction varies with dAGN separation. The black ‘+’ symbols indicate the fraction of all dAGNs that lead to a *LISA* SNR > 8. The right-hand panel shows how the fractions change when the effects of radiation feedback (RF) are taken into account (§ 5).

entire dAGN population (red circles) and the population that leads to *LISA* SNRs > 8 (black plus signs) closely follow the $M_{\text{sb}} = 10^{10} M_{\odot}$ results. This illustrates that galaxies with $M_{\text{sb}} \approx 10^{10} M_{\odot}$ dominate the sample of post-merger galaxies in TNG50-3. The right panel of Fig. 4 shows that the coalescence fraction of dAGNs with $q = 0.1$ and 0.5 have the highest coalescence fractions because the DF forces are larger (and the inspiral time shorter) for higher mass SMBHs (Li et al. 2020b, their Figure 11).

4.2. The Cumulative Coalescence Fractions of Dual AGNs

The results above focused on dAGNs that evolve to a MBH merger before $z_{\text{coal}} = 0$, but it is also interesting to examine how these mergers are distributed across redshift z_{coal} . Figure 5 shows the cumulative coalescence fractions (CCFs) of dAGNs with $L_{\text{bol}} > 10^{43} \text{ erg s}^{-1}$ at $z_{\text{dAGN}} = 1, 2$ and 3 .

The three lines in each panel shows the CCFs for dAGNs with different separations at the starting z_{dAGN} . Unsurprisingly, we see that dAGNs that start with a separation of only $a = 0.1 \text{ kpc}$ evolve to coalescence efficiently, reaching a 100% coalescence fraction by $z_{\text{coal}} \approx 0.9, 1.8, 2.6$, if starting at $z_{\text{dAGN}} = 1, 2$ and 3 , respectively. Similarly, 100% of the dAGNs with $a = 0.4 \text{ kpc}$ in our sample that are at $z_{\text{dAGN}} = 2$ or 3 merge by $z_{\text{coal}} \approx 1.2$ and 2.2 . Our calculations suggest that there may still be a small fraction of the $z_{\text{dAGN}} = 1, a = 0.4 \text{ kpc}$ population at low z , but the majority of them would have merged by $z_{\text{coal}} \approx 0.8$. In contrast, Fig. 5 shows that dAGNs with separations of $a = 0.7 \text{ kpc}$ at $z_{\text{dAGN}} = 1$ or 2 will not all have merged by $z_{\text{coal}} = 0$ although the ones

starting at $z_{\text{dAGN}} = 3$ would all have merged by $z_{\text{coal}} \approx 0.4$. Of course, the dAGNs that remain at low redshifts will be at significantly smaller separations (e.g., Fig. 2).

As in Fig. 4, we show in Figure 6 how the CCFs vary with M_{sb} (upper panels) and q (lower panels). dAGNs of all separations are included in each curve, and the dashed lines show CCFs of those mergers with *LISA* SNRs > 8. We replace the $z_{\text{dAGN}} = 3$ panels with one at $z_{\text{dAGN}} = 0.1$ to more closely connect to observational searches for dAGNs.

In the upper-row of the figure, we see the same inverse relationship between M_{sb} and coalescence fractions as seen in Fig. 4. For example, $\sim 30\text{--}40\%$ of $z_{\text{dAGN}} = 0.1$ dAGNs in galaxies with $M_{\text{sb}} = 10^9 M_{\odot}$ bulges will have coalesced by $z_{\text{coal}} = 0$. However, if the dAGNs reside in post-merger galaxies with $M_{\text{sb}} > 10^{10} M_{\odot}$, then only $\sim 10\%$ will merge in a Hubble time. The fractions increase markedly when considering dual AGNs at higher redshifts, however the fraction never rises above 40% for dAGNs in the most massive bulges. In the bottom row of Fig. 6, we again see that MBH pairs with larger values of q will evolve faster and reach coalescence at higher z_{coal} than lower values of q . The implication of this is that the most likely population of dAGNs persisting to low redshift will be systems with $\log q \lesssim -2$ and in galaxies with $M_{\text{sb}} \gtrsim 10^{11} M_{\odot}$. However, as shown by the dashed lines, the strongest *LISA* signals will originate from MBH pairs evolving in lower mass bulges (see also Paper I).

5. THE IMPACT OF RADIATION FEEDBACK EFFECTS

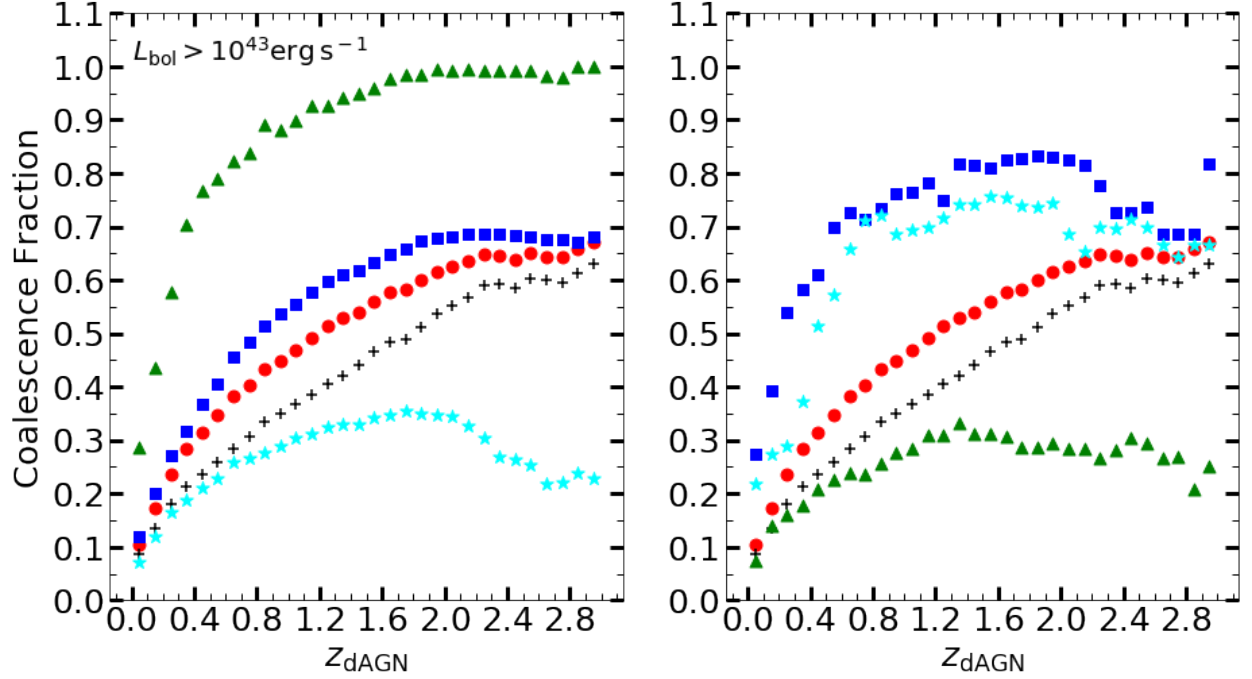


Figure 4. The fraction of dAGNs at a given redshift that coalesce by $z_{\text{coal}} = 0$. Left: the coalescence fraction of dAGNs grouped by the bulge mass. Green triangles represent systems with $\log(M_{\text{sb}}/M_{\odot}) = 9$, blue squares represent systems with $\log(M_{\text{sb}}/M_{\odot}) = 10$, and cyan stars represent systems with $\log(M_{\text{sb}}/M_{\odot}) = 11$. Right: the coalescence fraction of dAGNs grouped by the mass ratio q . Green triangles represent systems with $\log q = -2$, blue squares represent systems with $\log q = -1$, and cyan stars represent systems with $\log q = -0.3$. In both panels, red circles illustrate the coalescence fraction of all dAGNs, and the black plus signs represent the fraction of all dAGNs that coalesce by $z_{\text{coal}} = 0$ and can be detected by *LISA*.

The thermal pressure of the ionized bubble surrounding an accreting MBH regulates its accretion rate (e.g. Ostriker et al. 1976; Begelman 1985; Ricotti et al. 2008; Park & Ricotti 2011, 2012) and suppresses its luminosity. The magnitude of this effect depends on the motion of the MBH relative to its gas environment, the gas density, and the temperature of surrounding gas (Park & Ricotti 2013). Meanwhile, the ionized bubble can also reduce the DF force on MBHs moving in gas-rich hosts (Park & Bogdanović 2017; Gruzinov et al. 2020; Toyouchi et al. 2020), an effect known as “negative DF”. In several previous papers we showed that these radiation feedback (RF) effects may impact both the dAGN luminosities and the overall dynamical evolution of the sMBH (Li et al. 2020a, 2021, Paper I). In particular, Paper I showed that the negative DF effect increases the orbital decay timescale of sMBHs in gas-rich hosts, which could, in principle, severely reduce the expected *LISA* detection rates. In this section, we explore how RF will impact the evolution of the dAGN population. As the reduction in L_{bol} is relatively modest (RF does not typically impact the luminosity of the pMBH; Li et al. 2021), we focus here on the RF effects on the orbital decay of the sMBH. Details on how we implement RF in the calculation of the DF force can be found in the paper by Li et al. (2020a). We note that the RF effects are only computed during the DF phase of the MBH evolution, but, as seen Paper I, this phase dominates the overall timescale of a MBH merger.

Figure 7 shows the redshift distribution of all dAGNs in our model suite with $L_{\text{bol}} > 10^{43} \text{ erg s}^{-1}$ when the RF effects are included in the calculations. This plot should be compared to Fig. 1 which shows the results in the absence of RF. The green histogram shows the redshift distribution of all dAGNs and is similar to the one in Fig. 1, except that there are more dAGNs at $z \approx 0 - 0.4$ when RF effects are included. This is because negative DF slows the orbital decay, which results in longer evolution time and more dAGNs at low redshifts. Figure 7 also illustrates the redshift distribution of dAGNs with separations of $a = 0.7, 0.4$ and 0.1 kpc in the presence of RF. dAGNs separated by $a = 0.7$ kpc still dominate the population as in Fig. 1. However, when RF effects are included there are fewer dAGNs with separations of 0.4 and $a = 0.1$ kpc, especially at large redshifts. This is because negative DF increases the evolution time of most systems with gas fractions larger than 0.1 (Li et al. 2020a). Thus, it takes longer for most systems to reach smaller separations in the presence of RF, and thus, there are fewer dAGNs with separations < 0.4 kpc at high redshifts when RF is taken into account.

The impact of RF on the separation and luminosity distributions of all dAGNs that evolve to coalescence is shown in Figure 8 and should be compared to Fig. 2. Critically, the total number of systems that reach coalescence decreases in all panels when RF effects are included, with largest drop when

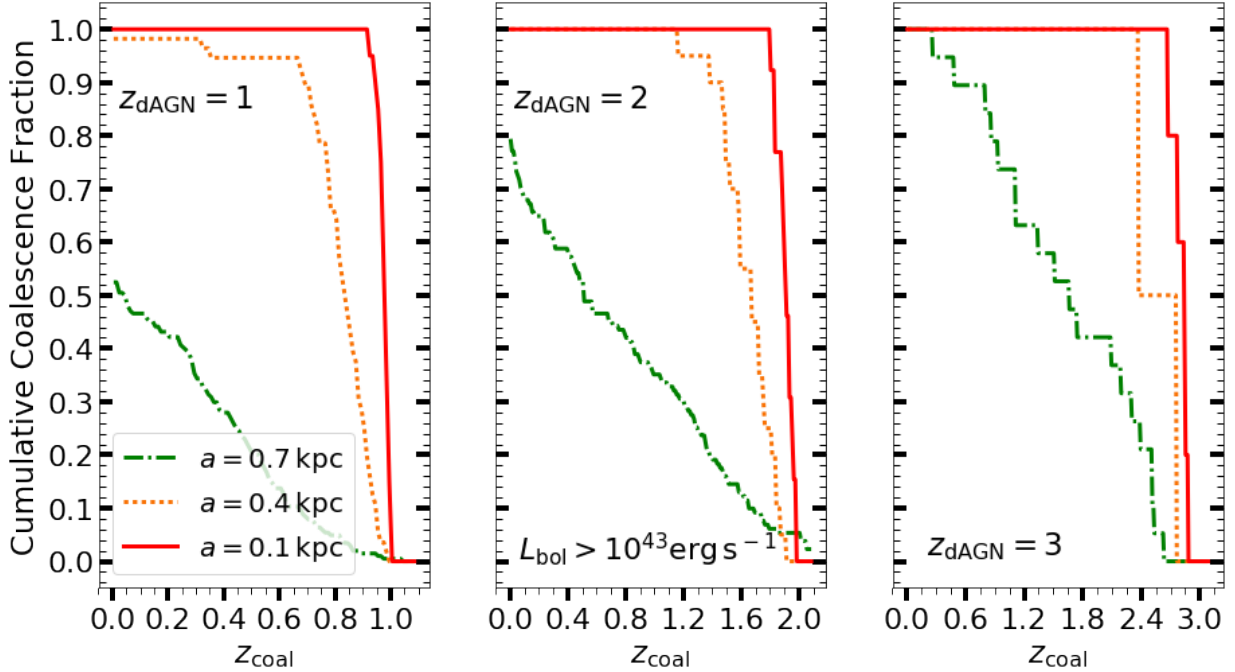


Figure 5. The cumulative coalescence fraction (CCF) of dAGNs with $L_{\text{bol}} > 10^{43} \text{ erg s}^{-1}$ at $z_{\text{dAGN}} = 1, 2$ and 3 . The dot-dashed green lines plot the CCFs of dAGNs with separations of $a = 0.7 \text{ kpc}$, while the dotted orange lines and solid red lines represent dAGNs with separations of 0.4 and 0.1 kpc , respectively.

$z_{\text{dAGN}} = 2$. This is a result of the increase in evolution time caused by RF effects (see Paper I). The shape of the separation distributions are largely similar between the two cases except for the one at $z_{\text{dAGN}} = 2$ which remains bimodal in the presence of RF, but the left peak at $a = 0.6 - 0.7 \text{ kpc}$ is now lower than the right peak at $a = 1.2 - 1.3 \text{ kpc}$, contrary to the outcome in the absence of RF. Dual AGNs with a separation of $0.6 - 0.7 \text{ kpc}$ at $z_{\text{dAGN}} = 2$ tend to have smaller binary masses and higher gas fractions compared to those dAGNs with the same separation but observed at $z_{\text{dAGN}} = 1$. Although the separation is the same, dAGNs at $z_{\text{dAGN}} = 2$ are more likely to stall in the presence of RF than those at $z_{\text{dAGN}} = 1$. So the left peak at $a = 0.6 - 0.7 \text{ kpc}$ is visibly reduced. The right peak at $a = 1.2 - 1.3 \text{ kpc}$ is largely due to dAGNs whose orbital evolution is determined by stellar DF in the bulge, which are also the ones that are least affected by RF, so the right peak is only slightly reduced in the presence of RF.

The bottom row of Figure 8 shows the bolometric luminosity distribution of all dAGNs that eventually coalesce in the presence of RF. Comparing this bottom row to the one in Fig. 2 we find that most dAGNs that evolve to mergers continue to have $L_{\text{bol}} = 10^{43-44} \text{ erg s}^{-1}$ at all z_{dAGN} in the presence of RF, but the total number of such systems has decreased significantly. However, the peak at $L_{\text{bol}} = 10^{45-46} \text{ erg s}^{-1}$ is barely affected by RF. This is because L_{bol} is proportional to the MBH pair mass, so the higher luminosity peak is composed of more massive dAGNs whose orbital evolution is determined by stellar DF in the bulge and is least affected by RF. Thus, the more luminous dAGNs are

barely affected by RF. The red-hatched histograms indicates systems that evolve to MBH mergers with $LISA \text{ SNR} > 8$. As these are concentrated in the lower mass, lower L_{bol} , systems, RF effects significantly decrease the number of these events (see also Paper I).

The impact of RF on the evolution of dAGNs is clearly seen in the right panel of Fig. 3 which shows the coalescence fraction of dAGNs with $L_{\text{bol}} > 10^{43} \text{ erg s}^{-1}$ as a function of z_{dAGN} in the presence of RF. Almost all dAGNs with separations of $a = 0.1 \text{ kpc}$ at $z_{\text{dAGN}} > 0.1$ coalesce before $z_{\text{coal}} = 0$, similar to the case in the absence of RF (the left panel of Fig. 3). However, there are no $a = 0.1 \text{ kpc}$ data points at $z_{\text{dAGN}} > 1.8$, since negative DF increases the evolution time, and none of our systems reaches $a = 0.1 \text{ kpc}$ at these redshifts. The square and star markers show the coalescence fraction of dAGNs with $a = 0.4$ and 0.7 kpc , respectively. Comparing to the coalescence fraction in the absence of RF as shown in the left panel of Fig. 3, at $z_{\text{dAGN}} < 1.8$, the coalescence fractions are in general reduced by 10–20% for $a = 0.4 \text{ kpc}$ dAGNs in the presence of RF, while for $a = 0.7 \text{ kpc}$ dAGNs the coalescence fraction is reduced by 30–50%. At $z_{\text{dAGN}} > 1.8$, the coalescence fractions are reduced significantly to 0.2–0.3 no matter the dAGN separation. This is because negative DF reduces the coalescence fraction.

Lastly, the red circles in the right panel of Fig. 3 represent the coalescence fraction of all dAGNs with $L_{\text{bol}} > 10^{43} \text{ erg s}^{-1}$ in the presence of RF. The coalescence fraction at $z_{\text{dAGN}} > 0.7$ is nearly flat, and corresponds to 0.2–0.25. Thus, in the presence of RF, if dAGNs are observed at

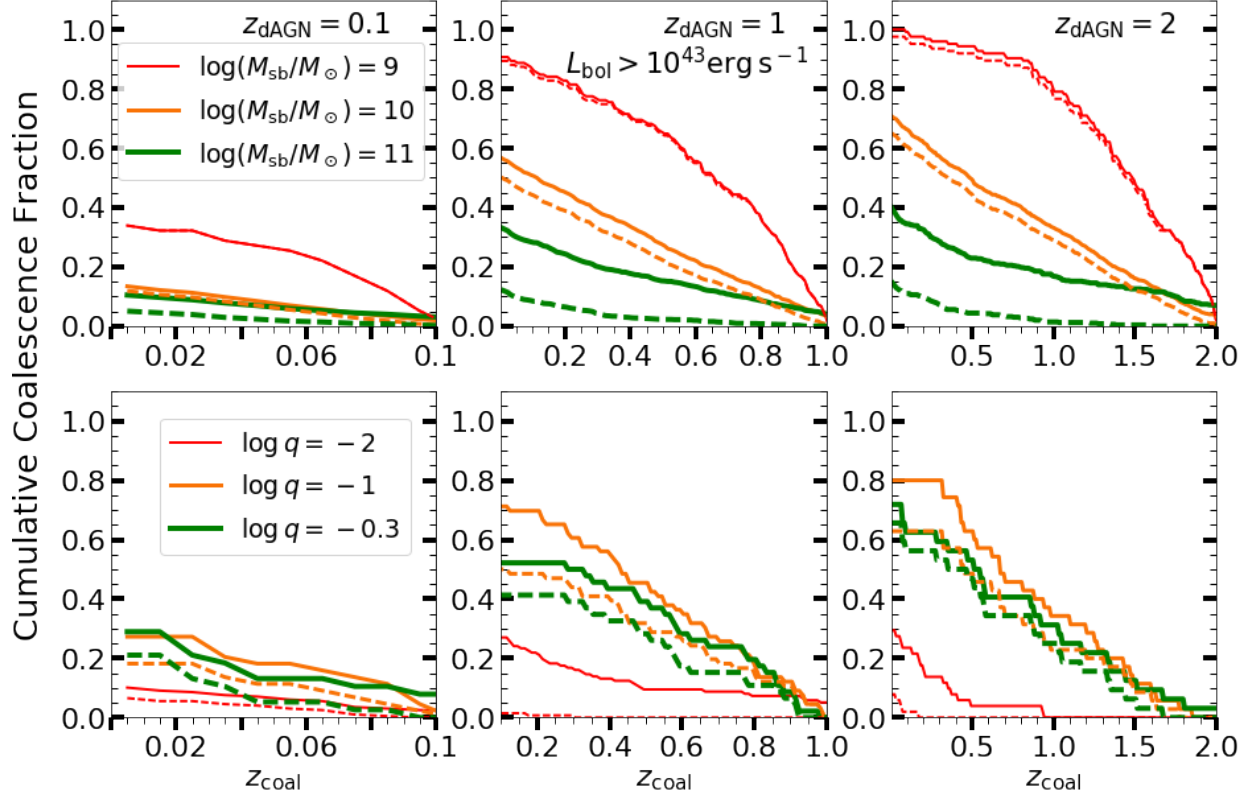


Figure 6. The cumulative coalescence fraction (CCFs) of dAGNs at $z_{\text{dAGN}} = 0.1, 1$ and 2 with $L_{\text{bol}} > 10^{43} \text{ erg s}^{-1}$ grouped by the stellar bulge mass (top row), and the MBH mass ratio (bottom row). The dashed lines show the CCFs of mergers that result in *LISA* events with $\text{SNR} > 8$.

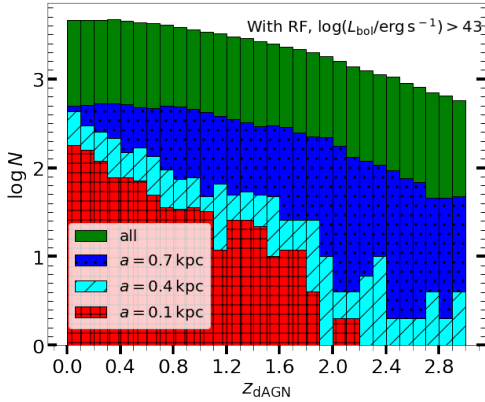


Figure 7. As Figure 1, but now showing the redshift distributions when including the effects of radiation feedback (RF).

$z_{\text{dAGN}} > 0.7$, then we expect 20–25% of them to coalesce by $z_{\text{coal}} = 0$. The black plus signs in this plot illustrate the the fraction of *LISA* GW sources in the presence of RF. Similar to the case in the absence of RF, the *LISA* detectable fraction of dAGNs is in general ~ 5 –10% lower than the total coalescence fraction.

6. DISCUSSION

6.1. Predicting the MBH Merger Rate from Dual AGN Surveys

The results presented above allow an estimate of the MBH merger rate, and the subsequent *LISA* detection rate, to be derived from an observational survey of kpc-scale dAGNs. Predictions can be calculated either in the presence or in the absence of RF effects. Given a survey of dAGNs with $L_{\text{bol}} > 10^{43} \text{ erg s}^{-1}$ at $z_{\text{dAGN}} \pm \Delta z$, the rate at which the MBHs in these systems merge before $z_{\text{coal}} = 0$ is

$$\frac{dN_{\text{coal}}}{dt}(z_{\text{dAGN}}) = f_{\text{coal}} n \frac{4\pi c d_L^2}{(1 + z_{\text{dAGN}})^2}, \quad (3)$$

where f_{coal} is the coalescence fraction at z_{dAGN} from Fig. 3, d_L is the luminosity distance to z_{dAGN} , and n is the observed dAGN comoving number density at z_{dAGN} . As an example, consider an all-sky survey that detected 400 kpc-scale dAGNs with $L_{\text{bol}} > 10^{43} \text{ erg s}^{-1}$ at $z_{\text{dAGN}} = 1 \pm 0.01$. Then

1. the dAGN comoving number density is $n = 400/4\pi d_L^2 c dt$. The time interval dt is the cosmological time across $z_{\text{dAGN}} = 1 \pm 0.01$ which is 0.081 Gyr in our adopted cosmology (see § 1).
2. According to the left panel of Fig. 3 the coalescence rate for dAGNs at $z_{\text{dAGN}} = 1$ in the absence of RF

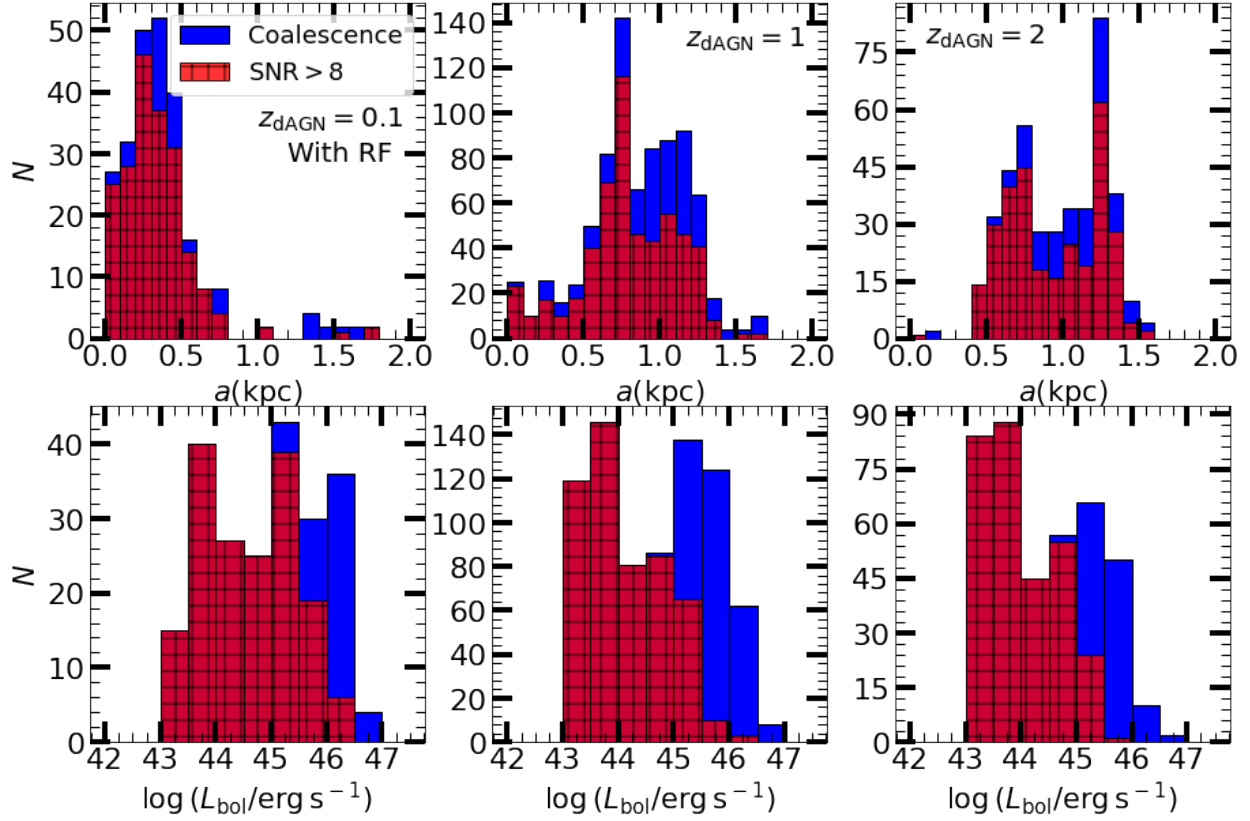


Figure 8. As Figure 2, but now showing the separation and luminosity distributions when RF effects are included.

effects is $f_{\text{coal}} \approx 0.45$. The fraction of dAGNs that lead to a merger with a *LISA* SNR > 8 is ≈ 0.35 .

3. The coalescence rate of these dAGNs at $z_{\text{dAGN}} = 1$ is found from Eq. 3: $dN_{\text{coal}}/dt \sim 6 \times 10^{-7} \text{ yr}^{-1}$. The rate of mergers with a *LISA* SNR > 8 is $\sim 5 \times 10^{-7} \text{ yr}^{-1}$.

To include the effects of RF, the calculation can be repeated using the values of f_{coal} from the right-hand panel of Fig. 3. In the example above, RF reduces the predicted merger rates to $3 \times 10^{-7} \text{ yr}^{-1}$ (all systems) and $2 \times 10^{-7} \text{ yr}^{-1}$ (those with *LISA* SNR > 8).

Eq. 3 gives the expected rate of MBH mergers from a population of dAGNs at a particular z_{dAGN} . If this estimate can be made at multiple z_{dAGN} the results can be integrated to yield the total MBH merger rate. In Paper I we found that the overall MBH coalescence rate is $\sim 0.45 \text{ yr}^{-1}$ in the absence of RF effects, while the rate of sources with a *LISA* SNR > 8 is $\sim 0.34 \text{ yr}^{-1}$. Comparing the merger rates derived from dAGN observations and Eq. 3 with future *LISA* measurements will provide important constraints on the efficiency of DF forces and RF effects in the orbital evolution of MBH pairs.

6.2. Comparison to Results from Literature

In the paper by Volonteri et al. (2021), dAGNs in the cosmological simulation *Horizon-AGN* are identified and related

to the corresponding MBH binary mergers from the same simulation (Volonteri et al. 2020), and the numerical relation between the dAGNs and MBHB mergers is studied. The right column of their Figure 11 illustrates the CCFs of dAGNs with 5 ~ 10 kpc separations. According to their results, 30 – 60% of these dAGNs observed at $z_{\text{dAGN}} \sim 1 - 3$ coalesce before $z_{\text{coal}} = 0$, increasing with decreasing z_{dAGN} . This is due to the long evolution time of dAGNs with small mass ratios at high redshifts. These high redshift dAGNs with small mass ratios are formed in *Horizon-AGN* simulation because the criterion for MBH formation is based only on gas properties. Thus, at high redshifts, when the gas reservoir is rich, some MBHs form in gas clouds that are too small to be identified as galaxies (‘intergalactic’ MBHs). These small ‘intergalactic’ MBHs can be captured by galaxies later on and shine as dAGNs if some stochastic accretion occurs (Volonteri et al. 2021). According to the left column of Figure 11 of Volonteri et al. (2021), dAGNs with one ‘intergalactic’ MBH have small mass ratios and occur frequently at high redshifts (20 ~ 30% of all dAGNs at $z = 2, 3$). The evolution time of these systems is long and the resulting coalescence fractions are low due to the small mass ratios, which leads to low coalescence fractions of dAGNs at high redshifts as shown in the right column of their Figure 11.

In comparison with Figure 5 of this paper, the CCFs in Volonteri et al. (2021) are in general lower at all z_{dAGN} . This is because the initial dAGN separations considered in

Volonteri et al. (2021, 30 – 50 kpc) are larger than that considered in this work (\sim kpc), so the evolution time is longer and CCFs are lower in their case. As shown in Figure 5, the CCFs increase with increasing z_{dAGN} , contrary to the results of Volonteri et al. (2021). This is because we do not include those systems comprising one ‘intergalactic’ MBH in the analysis of this work (see § 3 of paper I). Overall, the results of Volonteri et al. (2021) indicate dAGNs that are identified at small separations are generally indicators of effective mergers, which is in agreement with our results.

6.3. Impact of Simplifying Assumptions

The advantage of our semi-analytic model is its ability to provide calculations over a wide range of galaxy and MBH orbital properties at the cost of making some simplifying assumptions. The potential impact of our assumptions on the dynamical evolution of MBH pairs is discussed by Li et al. (2020b,a, Paper I). In this section, we consider the possible effects of these assumptions on the dAGN properties and their connection to MBH mergers.

We assume that the pMBH is fixed at the center of the host galaxy. If the motion of the pMBH and its corresponding Bondi-Hoyle-Lyttleton accretion rate are accounted for in the calculations, the resulting bolometric luminosity would be lower and the evolution time would be shorter. In this case, there would be fewer dAGNs with $L_{\text{bol}} > 10^{43}$ erg s $^{-1}$ and more MBH mergers at higher redshift, resulting in a larger coalescence fraction of dAGNs. Consequently, including the motion of the pMBH would increase the *LISA* detection rate. This effect would be strongest in comparable mass MBH pairs and weaker in those with small q . It would be manifested as an increase in the number of high redshift *LISA* detections, since MBH pairs at high redshifts tend to have larger mass ratios.

The orbit of the sMBH is assumed to always reside in the midplane of the model remnant galaxy. If an inclined orbit takes the sMBH outside of the galactic gas disk, the evolution time would increase and L_{bol} would decrease. We also assume that the sMBHs do not grow in mass during their orbital evolution from kpc scales toward coalescence. Had they been able to do so, the increase in the total mass of the binary would render the inspiral time shorter and their bolometric luminosity higher.

As mentioned in § 5, we considered the effect of RF only during the DF phase. Some studies have shown that RF can also affect the orbital evolution of sMBHs in circumbinary disks if there is no gap formed. Especially when sMBHs accrete at high rates, the radiation leads to strong winds pushing against the gas disk, blowing the gas away from the binary which stalls the binary hardening in the circumbinary disks (del Valle & Volonteri 2018; Williamson et al. 2022). On the contrary, when there is a gap in the disk, RF does not affect the evolution time of sMBHs (del Valle & Volonteri 2018). Our model assumes the gap-opening regime (Paper I), so taking into account RF in circumbinary disks should not significantly affect the dAGN coalescence fraction and the *LISA* detection fraction predicted in this work.

Triplets of MBHs are likely to form at high redshifts, when the merger rate of galaxies is high. MBHs in these triplets may undergo the Kozai-Lidov oscillations which may increase the eccentricity of the central MBHBs (Kozai 1962) and increase the dAGN coalescence rate. Besides the Kozai-Lidov oscillations, the chaotic three-body interactions can also boost the coalescence rate (Blaes et al. 2002; Hoffman & Loeb 2007; Amaro-Seoane et al. 2010; Kulkarni & Loeb 2012; Bonetti et al. 2016; Ryu et al. 2018). If triplets and the three-body interactions were included in our model, the dAGN coalescence fractions and the *LISA* detection fraction would be higher.

We do not take into account gas consumption and star formation in the merger remnant galaxies. This means that during the orbital evolution from \sim kpc to coalescence, the gas fraction of a host remains at the same value inherited from TNG50-3 data file. This assumption potentially increases the number of dAGNs with $L_{\text{bol}} > 10^{43}$ erg s $^{-1}$, since in reality at least a fraction of the gas reservoir turns into stars. This reduces the gas fraction and increases the stellar density in the host galaxies. In the presence of RF, higher stellar densities result in more efficient orbital evolution of MBH pairs and more MBH mergers. Thus, in the presence of RF the coalescence fraction of dAGNs would be higher than determined here. In the absence of RF, the effect of this assumption can not be easily predicted due to the complicated interplay of DF and the galactic parameters (Li et al. 2020b). The host galaxies with high gas fraction are affected most by this assumption.

7. CONCLUSIONS

dAGNs are a product of galaxy mergers and trace the population of future MBH coalescences. In this paper, we combined the MBH dynamical evolution calculations from Paper I with estimates of AGN luminosity to explore how the luminosities and separations of dAGNs change as the MBH pair evolves in its host galaxy. In addition, we were able to calculate the fraction of the dAGN population at a redshift z_{dAGN} that lead to a MBH merger at redshift z_{coal} , including determining the fraction that lead to a *LISA* SNR > 8 .

We find that, in the absence of RF effects, the dAGN population in our model, with total bolometric luminosity $L_{\text{bol}} > 10^{43}$ erg s $^{-1}$, peaks at $z_{\text{dAGN}} \approx 0.4$ and is dominated by systems with separations $a \gtrsim 0.7$ kpc (Fig. 1). However, a majority of these dAGNs will not lead to MBH mergers before $z_{\text{coal}} = 0$ (Fig. 3). In fact, the majority of low- z_{dAGN} dAGNs that are precursors to MBH mergers are separated by $\lesssim 0.5$ kpc (Fig. 2). This is a result of the orbital decay times of the sMBH—there is simply not enough time for most $a \sim 0.7$ kpc dAGNs at $z_{\text{dAGN}} \approx 0.4$ to evolve through to coalescence before $z_{\text{coal}} = 0$. Therefore, a closer connection between dAGNs and MBH mergers can be most easily obtained by detecting dAGNs at $z_{\text{dAGN}} \gtrsim 1$, where the coalescence fraction exceeds 0.5. The separation of dAGNs at $z_{\text{dAGN}} \gtrsim 1$ is ~ 0.7 – 1 kpc and the total $L_{\text{bol}} \approx 10^{43-46}$ erg s $^{-1}$.

The orbital evolution of the sMBH depends on the properties of the post-merger galaxy and MBH pair (e.g., Li et al.

2020b, Paper I), so these conditions also impact the coalescence fractions of dAGNs. We find that dAGNs in post-merger galaxies with bulge masses $M_{\text{sb}} \lesssim 10^{10} M_{\odot}$ and with MBH mass ratios of $q \approx 0.5$ have the highest coalescence fractions. The fractions increase with z , observational searches for dAGNs that lead to MBH mergers may consider prioritizing galaxies with less massive stellar bulges.

In Paper I we found the radiation feedback effects can significantly increase the evolution timescales for MBH pairs, in particular in high gas fraction galaxies. This phenomenon (“negative DF”) leads to a drop in the expected MBH coalescence rate and is seen in the dAGN properties when we include this effect (Fig. 3 and 8). A signature of RF effects is in a larger than expected number of dAGNs with wide separations, as this would indicate slow orbital decay predicted by negative DF.

The coalescence fractions shown in Fig. 3 can be combined with the results of dAGN surveys to predict both the MBH merger rate and the rate of *LISA* signals with $\text{SNR} > 8$. We provide a recipe in § 6.1 that can be followed to calculate these rates (either with or without RF effects) from observations of dAGNs. Comparing these predicted rates to *LISA* measurements can be used to test our understanding of DF, including the importance of RF effects. The results like the ones presented here, in combination with the next-generation of dAGN surveys, will thus be crucial in testing the physical models of MBH evolution at sub-kpc scales.

ACKNOWLEDGMENTS

T.B. acknowledges the support by the National Aeronautics and Space Administration (NASA) under award No. 80NSSC19K0319 and by the National Science Foundation (NSF) under award No. 1908042.

REFERENCES

- Amaro-Seoane, P., Sesana, A., Hoffman, L., et al. 2010, *MNRAS*, 402, 2308
- Amaro-Seoane, P., Audley, H., Babak, S., et al. 2017, arXiv e-prints, arXiv:1702.00786
- Antonini, F., & Merritt, D. 2012, *ApJ*, 745, 83
- Armitage, P. J., & Natarajan, P. 2005, *ApJ*, 634, 921
- Barausse, E. 2012, *MNRAS*, 423, 2533
- Begelman, M. C. 1985, *ApJ*, 297, 492
- Begelman, M. C., Blandford, R. D., & Rees, M. J. 1980, *Nature*, 287, 307
- Binney, J., & Tremaine, S. 2008, *Galactic Dynamics: Second Edition* (Princeton University Press)
- Blaes, O., Lee, M. H., & Socrates, A. 2002, *ApJ*, 578, 775
- Bondi, H. 1952, *MNRAS*, 112, 195
- Bondi, H., & Hoyle, F. 1944, *MNRAS*, 104, 273
- Bonetti, M., Haardt, F., Sesana, A., & Barausse, E. 2016, *MNRAS*, 461, 4419
- Bonetti, M., Sesana, A., Haardt, F., Barausse, E., & Colpi, M. 2019, *MNRAS*, 486, 4044
- Chandrasekhar, S. 1943, *ApJ*, 97, 255
- De Rosa, A., Vignali, C., Bogdanović, T., et al. 2020, arXiv e-prints, arXiv:2001.06293
- del Valle, L., & Volonteri, M. 2018, *MNRAS*, 480, 439
- Gruzinov, A., Levin, Y., & Matzner, C. D. 2020, *MNRAS*, 492, 2755
- Hoffman, L., & Loeb, A. 2007, *MNRAS*, 377, 957
- Hoyle, F., & Lyttleton, R. A. 1939, *Proceedings of the Cambridge Philosophical Society*, 35, 405
- Kelley, L., Charisi, M., Burke-Spolaor, S., et al. 2019, *BAAS*, 51, 490
- Kelley, L. Z., Blecha, L., & Hernquist, L. 2017, *MNRAS*, 464, 3131
- Khan, F. M., Awais Mirza, M., & Holley-Bockelmann, K. 2019, arXiv e-prints, arXiv:1911.07946
- Kim, H., & Kim, W.-T. 2007, *ApJ*, 665, 432
- Kozai, Y. 1962, *AJ*, 67, 591
- Kulkarni, G., & Loeb, A. 2012, *MNRAS*, 422, 1306
- Li, K., Ballantyne, D. R., & Bogdanović, T. 2021, *ApJ*, 916, 110
- Li, K., Bogdanović, T., & Ballantyne, D. R. 2020a, *ApJ*, 905, 123
- , 2020b, *ApJ*, 896, 113
- Li, K., Bogdanović, T., Ballantyne, D. R., & Bonetti, M. 2022, *ApJ*, 933, 104
- Lusso, E., Comastri, A., Simmons, B. D., et al. 2012, *MNRAS*, 425, 623
- Milosavljević, M., & Phinney, E. S. 2005, *ApJL*, 622, L93
- Nelson, D., Springel, V., Pillepich, A., et al. 2019a, *Computational Astrophysics and Cosmology*, 6, 2
- Nelson, D., Pillepich, A., Springel, V., et al. 2019b, *MNRAS*, 490, 3234
- Ostriker, E. C. 1999, *ApJ*, 513, 252
- Ostriker, J. P., McCray, R., Weaver, R., & Yahil, A. 1976, *ApJL*, 208, L61
- Park, K., & Bogdanović, T. 2017, *ApJ*, 838, 103
- Park, K., & Ricotti, M. 2011, *ApJ*, 739, 2
- , 2012, *ApJ*, 747, 9
- , 2013, *ApJ*, 767, 163
- Pillepich, A., Nelson, D., Springel, V., et al. 2019, *MNRAS*, 490, 3196
- Quinlan, G. D. 1996, *NewA*, 1, 35
- Quinlan, G. D., & Hernquist, L. 1997, *NewA*, 2, 533

- Ricotti, M., Ostriker, J. P., & Mack, K. J. 2008, *ApJ*, 680, 829
- Ryu, T., Perna, R., Haiman, Z., Ostriker, J. P., & Stone, N. C. 2018, *MNRAS*, 473, 3410
- Thorne, K. S., & Braginskii, V. B. 1976, *ApJL*, 204, L1
- Toomre, A. 1964, *ApJ*, 139, 1217
- Toyouchi, D., Hosokawa, T., Sugimura, K., & Kuiper, R. 2020, *MNRAS*, arXiv:2002.08017
- Valiante, R., Schneider, R., Volonteri, M., & Omukai, K. 2016, *MNRAS*, 457, 3356
- Volonteri, M., Haardt, F., & Madau, P. 2003, *ApJ*, 582, 559
- Volonteri, M., Pfister, H., Beckmann, R., et al. 2021, arXiv e-prints, arXiv:2112.07193
- Volonteri, M., Pfister, H., Beckmann, R. S., et al. 2020, *MNRAS*, 498, 2219
- Williamson, D. J., Bösch, L. H., & Hönig, S. F. 2022, *MNRAS*, 510, 5963
- Yu, Q. 2002, *MNRAS*, 331, 935